Pre-print of the article
M. Pesenti, G. Masera, F. Fiorito, Exploration of Adaptive Origami Shading Concepts through Integrated Dynamic Simulations, Journal of Architectural Engineering, volume 24, issue 4, December 2018, page 04018022.
DOI: 10.1061/(ASCE)AE.1943-5568.0000323
AE662 Available at https://ascelibrary.org/doi/abs/10.1061/%28ASCE%29AE.1943-5568.0000323

Exploration of Adaptive Origami Shading Concepts through Integrated Dynamic Simulations

Marco Pesenti[a], Gabriele Masera[b], Francesco Fiorito[c]

[a] Department of Architecture, Built Environment and Construction Engineering, Politecnico di Milano, 20133 Milano, Italy. E-mail: marco.pesenti@polimi.it.
[b] Department of Architecture, Built Environment and Construction Engineering, Politecnico di Milano, 20133 Milano, Italy. E-mail: gabriele.masera@polimi.it.
[c] Department of Civil, Environmental, Land, Building Engineering and Chemistry, Politecnico di Bari, 70125 Bari, Italy. E-mail: francesco.fiorito@poliba.it.

Abstract

The paper presents integrated energy and lighting simulations as a part of a wider research focused on the form-finding process of adaptive shading concepts and on the actuation of their movement using Shape Memory Alloys (SMAs). The use of this new type of micro-actuators in responsive architectural components represents a challenge because of their limited contraction state. Origami shapes have been, therefore, considered to amplify the movement thanks to their geometric properties. The paper exploits visual and thermal comfort of a south oriented office located in Milan (Italy) and equipped with an adaptive Origami shading. Two-hundred and ten shapes have been considered and geometry, contraction state and surface materials have been considered as variable properties. The final aim was to explore the potential of adaptive Origami shadings in controlling visual and thermal comfort. Useful Daylight Illuminance (UDI), Daylight Glare Probability (DGP) and Total Energy (TE) demand (cooling, heating and lighting per year) have been used as main metrics for understanding environmental benefits of the proposed shading devices.

Keywords: Origami shapes; adaptive shading device; dynamic simulation; visual comfort; energy consumption.

Introduction

The performances of building envelopes are crucial to reduce the energy consumption of buildings, which consume an estimated 40% of the overall energy used worldwide (Janssen 2004). Recently, the more restrictive European energy policies in terms of energy efficiency (Directive 2010/31/EU) saw building performance requirements increase. On this trend, the concepts of nearly Zero Energy Buildings (n-ZEBs) or positive-energy buildings (PEBs) have been introduced. New design concepts have been, then, proposed based on the improvement of building fabric, on the use of innovative shading devices, on the integration of high performance Heating, Ventilation and Air Conditioning (HVAC) systems, and on the adoption of advanced control sensors (Kolokotsa et al. 2011). New envelopes' typologies have been introduced in order to: (a) minimize the energy consumption adopting a passive approach, and (b) balance the energy production by means of renewable energy systems. Orientation, building shape, window to wall ratio (WWR), insulation levels, shading, and integration of innovative and high-performance materials are some of the foundation criteria of the passive approach. Several studies focus on passive solutions, considered more reliable and easy to implement than active ones (Pacheco et al. 2012). Moreover, these strategies do not need complex control systems. Several studies are reported in literature on adaptive technologies for the building envelope, such as Climate Adaptive Building Shells (CABS) (Loonen et al. 2013) and Acclimated Kinetic Envelope (AKE) (Wang et al. 2012). Adaptive envelopes are composed of dynamic sub-components able to change properties in a reversible manner, reacting to one or more external stimuli. Within the envelope, adaptive technologies find an interesting niche of application in windows. Smart chromogenic glasses (Baetens et al. 2010; Granqvist 2002; Jelle et al. 2012; Malara et al. 2014), integrated smart facades (Jones et al. 2015),

thermally adaptable windows (Goia et al. 2014) and movable shading systems (Adriaenssens et al. 2014; Lienhard et al. 2011; Suralkar 2011) are some of the recently developed technologies.

As main goals of our research are to reduce the complexity of the movement and to create an adaptive component, Shape Memory Alloy (SMA) micro actuators have been selected to control the shape's change in direct response to the incoming solar radiation. Multi-faced Origami shapes have been analysed due to their capability to amplify movements, providing good deployment ratios with limited actuators' displacement. Furthermore, the use of Origami allows the integration of different materials simultaneously, providing alternative solutions customisable based on requirements. Origami geometries used as shading devices are, then, tested through dynamic visual and thermal simulations. Daylight Glare Probability (DGP), Useful Daylight Illuminance (UDI), Daylight Autonomy (DA) and Total Energy consumption (TE) have been used to describe the effects of shadings' movement and to select the most promising shape patterns.

Aims and limitations: Origami patterns and the use of SMAs micro-actuators

Origami patterns as deployable surfaces have already shown their potential for application in kinetic shading devices. Since the 1980s, several Origami-inspired structures have been used in architecture. Recently an Origami-shaped responsive facade coupled with mechanical actuators was used in the Al-Bahar towers in Abu Dhabi (Aedas 2012), while Cheng et al. (2012a; 2012b) developed and tested several Origami-shaped sun-shades.

The present study investigates the kinetic nature of Origami shapes, derived from their particular geometry. Origami are constituted of creases that fold along pre-set directions while showing a rigid behaviour along the others. In particular, rigid Origami surfaces are based on a series of valley and mountain creases connected by folds that act like hinges. Through these, the surface contracts and expands to find stability (Osório et al. 2014). This intrinsic anisotropy results

in a change of shape into a stable configuration. The final shape is the one that minimises internal tensions maintaining the external surface continuous without stretching the material.

Given the embedded characteristics of Origami shapes, the integration with smart actuators is envisaged as one of the potential exploration paths. Compared to a standard adjustable system, one the benefits of such a strategy lay in the reduction of mechanical complexity and, consequently, of the energy required to trigger the movement. SMAs have been chosen, among smart actuators, for their weather resistance, overall durability, and low activation energy (Nespoli et al. 2010).

SMA wires and springs have been previously tested in order to derive their mechanical properties and, thus, to compare the products available on the market. Studies previously conducted by the authors (2015b) have examined mechanical properties of wires and springs under different conditions of use. SMA springs demonstrate higher percentage of contraction and their use was further explored in this paper. Fig. 1 shows a preliminary test carried out on the SMA spring that we selected as shape change actuator for the adaptive shading device. The SMA spring has a length of 140 mm and 29 mm respectively in its maximum elongation and in its maximum contraction. In the test, the SMA spring is attached to a bias spring and its movement is triggered by electricity. The test was used to calculate the contraction time (31 s) and the elongation time (165 s). The difference between contraction and elongation time is due to the hysteresis, typical of the material (Fiorito et al. 2016).

In order to understand how geometries and actuators can be coupled to find an optimised range of folding, the deployment of Origami patterns at the global scale has been examined. Five Origami patterns have been here considered and modelled in a standard test room. The overarching aims are: a) to define the Origami pattern with the highest performance as external shading system and

b) to define the overall benefits in terms of visual and thermal comfort achievable with monthly, daily or hourly movements of the shading.

Simulating an adaptive envelope: a review

Visual comfort indicators and total energy consumption should be simultaneously considered to properly account for benefits associated with adaptive building envelopes. Performance indicators are therefore needed to evaluate options in a multi-criteria selection environment (Jin and Overend 2014). Simulation-based approaches increase the opportunity to envision techniques and products tested through whole-building performance simulation together with sensitivity analyses and iterative evaluations of product variation. To account for all these factors at once, daylight and thermal simulations started to be coupled by defining a series of metrics that describe daylight levels inside the space and its ability to reduce the energy consumption (Lee et al. 2004; Manzan and Padovan 2015; Tzempelikos and Athienitis 2007).

The introduction of daylighting strategies as design parameter to reduce cooling and artificial lighting demand highlighted the significant relationship between light and energy (Koo et al. 2010; Lollini et al. 2010). Now more than ever, simulations are becoming an important step to develop product potentials in a cost-effective way. Thanks to simulations with pre-set performance indicators, the envelope can be analysed in different climatic conditions (Loonen et al. 2014) and results vary based on the choice of parameters (Lohnert et al. 2003).

Window to Wall Ratio (WWR) has been widely used as a parameter to assess the balance between daylight availability and energy savings. A WWR threshold of 40% has been described as sufficient for daylight comfort levels by Pellegrino et al. (2015), while Goia et al. (2013) underlined how WWR in a low-energy office building is a parameter that scarcely influences the total energy demand. In case of high WWR, however, external shading devices have shown to be

the most effective way to control simultaneously daylight and solar gains. One of the first studies on the integration of static and dynamic shading devices in office buildings (Tzempelikos and Athienitis 2007) demonstrated that a reduction of up to 12% of the total energy demand could be reached by using a proper strategy of windows' shading, in comparison to a solution without shadings.

High-performance facades integrated with adjustable elements require more accurate and detailed information during the design process. Thus, instead of collecting data from simplified methods and tools based on steady-state conditions, annual dynamic simulations can reduce the risk of performance gaps between design and operations.

Hammad and Abu-Hijleh (2010) have compared dynamic and static blinds in terms of shapes and material properties using light dimming methodology and working on the total combined solar heat gain coefficient. Following that, Nielsen et al. have evaluated the potentialities of these systems, thought as changeable throughout the year (Nielsen et al. 2011). By integrating daylighting and energy simulations, the authors demonstrated how the interdependence between parameters produces better performances in comparison to the ones of a static facade. To understand the relation between shape and function, parametric modelling tools are increasingly adopted within the design process and for research purposes to optimise the workflow (Hammad and Abu-Hijleh 2010; Naboni 2014).

According to Sartori et al. (2012), annual based simulations are suitable to cope building balances with variations of meteorological conditions. Furthermore, quasi-static or dynamic calculations, like seasonal and daily-based ones, could help in optimizing the interactions between buildings and the surrounding environment. A variety of studies proposed methods and tools to analyse adaptive building facades, especially highlighting the potential annual, monthly and daily

energy savings. The method described by Kasinalis et al. (2014) included a sequence of multi-objective optimisation scenarios to envision the optimal seasonal adaptation strategies. In continental climatic conditions, a monthly adaptation of the south facade can reduce of up to 15% the building energy demand. The improvement of thermal conditions due to the use of an adaptive façade in comparison with a fixed one was another benefit highlighted by the authors. Similar remarks have been underlined by Favoino et al. (2015), where the variation of glazing properties and WWR for three different locations (Helsinki, London and Rome) produced savings up to 20% monthly. The research simulated also the same facades on daily-basis adaptability, finding 30% energy saving with respect to the reference facade.

Methodology

Definition of the standard reference room

A room, representative of a double occupancy office, has been considered as reference for the performance assessment of dynamic Origami shadings. The room is supposed to be located in Milan (Italy, 45°37' N, 8°43' E) as part of a cluster unit in a middle-size office building. The hourly weather data come from the Milan IWEC file, collected from the U.S. Department of Energy's (DOE) database.

Only the south façade of the room is exposed to external boundary conditions, whilst the remaining surfaces are close to an adiabatic condition. In order to enable the comparison of the results provided in this paper with studies that can be found in existing literature, room dimensions, construction details and the office layout follow some of the reference building specifications suggested by van Dijk (2002).

Specific envelope requirements have been defined according to the most recent Italian regulation on energy efficiency in buildings (Italy 2013). More specifically, the thermal

transmittance (U-value) of external walls (oriented to south) is 0.176 W/m^{2}K. Windows are composed of Double Glazing Units (DGU), with a U-value of 1.41 W/m^{2}K, Visible Light Transmittance (VLT) of 0.68, and Solar Heat Gain Coefficient (SHGC) of 0.49. In line with current trends in the design of office buildings and the façade layout proposed by van Dijk (2002), the external wall has a WWR slightly higher than 60%.

Reflectance (R) values of opaque surfaces have been assumed 0.2 for external ground, interior floor and desk surface, 0.5 for internal walls and partitions, and 0.8 for the ceiling. Specularity (S) and roughness (ρ) values of 0 have been associated to all surfaces, so as to consider them perfectly diffusive and, thus, able to homogeneously reflect the light.

The office has a double occupancy, generating an internal gain of 120 W/p, due to sensible and latent heat emission. Equipment and artificial lighting have been set at 10 W/m^2 and 12 W/m^2 respectively. Artificial lighting systems have been modelled as linearly dimmable, controlled by illuminance sensors. A horizontal illuminance threshold on the work plane of 500 lx has been considered to be reached by the combination of natural and artificial lighting.

An ideal HVAC system supplies heating, cooling and artificial ventilation. This system has been considered active only during the hours of occupation, with set point temperatures of 20°C for heating and 24°C for cooling. HVAC's Coefficients of Performance (COP) are 3.5 and 2.5 respectively for heating and cooling. Furthermore, a constant rate of ventilation of 3.26 Air Changes per Hour (ACH) has been considered (1.5 ACH of fabric infiltration, plus 0.88 ACH/p of fresh air intake) according to the UNI 10339: 1995 (1995).

Two reference surfaces (P1 and P2) have been assumed. They correspond to position of each of the two desks and therefore they are placed at a height of 0.8 m from the floor. The choice has been made intentionally to highlight what happens when the worst scenario is considered. Figure

1. The shape memory alloy spring is activated using a power supply. At the bottom right of each image the time of contraction and then elongation is displayed.

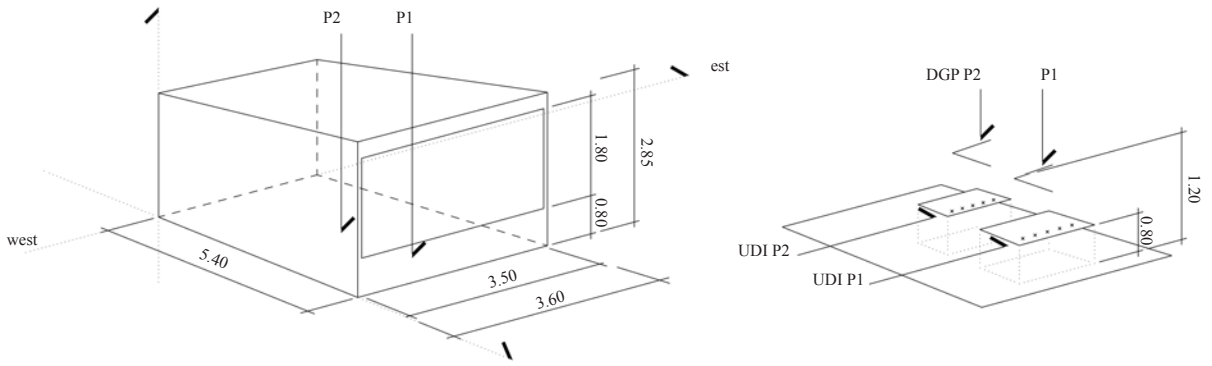

Figure (b) includes the detailed position of reference points used for illuminance and glare calculations. For each reference surface, five illuminance sensors (measuring horizontal illuminance), evenly distributed on the surface at a mutual distance of 0.35 m, have been considered. The spacing between sensors has been decided as to point out the effects on illuminance distribution due to the complex three-dimensional geometry of the Origami patterns. This approach allowed to monitor the reliability of the illuminance values obtained. Glare indexes have been calculated for two viewpoints. The viewpoints are pointing directly towards the centre of the window, at distances of 1.7 m and 3.7 m respectively. The viewpoints represent users in a seated position, therefore considering the eye level at 1.2 m from the floor.

While P1 location has been mainly used for assessing visual comfort (in terms of both glare and useful daylight illuminance) because of its proximity with the window, P2 location has been used to evaluate the worst-case scenario for internal daylight illuminance. Therefore, hourly artificial

lighting schedules have been defined according to average horizontal illuminance values collected from location P2.

Shaping the shading device: the use of Origami patterns

Five combinations of patterns and actuators have been then selected, due to their high efficiency in movement. As highlighted by Pesenti et al. (2015b; 2015a), a contraction in the range of 10-25% has been found to be capable of activating self-folding properties. Besides, this range becomes feasible if SMA springs are taken into account.

A folding rate at 25% of contraction (FR_{25}) has been used for assessing the performance of the analysed Origami families. It is defined as:

$$FR_{25} = \frac{A_i - A_{25}}{A_i}, \quad (1)$$

where A_i is a projection on a vertical plan (the facade's) of the undeformed pattern, and A_{25} is the projection on vertical plan of the deformed pattern with an actuator contraction state of 25%.

Figure summarises deployment direction, actuators arrangement and folding percentages for five of the most promising Origami geometries.

Due to its modular nature, the Ron Resch pattern (RR) performed better with actuators arranged along the projection of the folding creases. The placement of actuators as hexagons connecting the valleys intersection results in a FR_{25} of 44% with an additional displacement along the normal to the surface. Similarly, the Waterbomb pattern (WB) showed promising percentages of folding if the actuators are placed along a uniform square grid. With a FR_{25} of 43%, Waterbomb is one of the most interesting patterns, which develops, similarly to Ron Resch, a dome-like shape when contracted. Glide Reflection patterns (GR, GR2) are characterised by moduli of variable dimensions. Thanks to this property, they are able to achieve very high percentage of folding (48%) among the five selected patterns. Finally, the modular Miura Ori pattern (MO) has been considered

because of its dynamic nature. Module variation, bi-dimensional deployment and free deformation in the three directions are some of its main properties.

In order to modulate the shadings' transparency, two separate faces have been defined for each of the five patterns, as can be seen in Figure . Their geometric relationship depends on the specific pattern considered. While Glide reflection 2 and Miura Ori patterns (GR2, MO) have an equal distribution of A and B faces (geometric ratio of 1), Ron Resch (RR) and Waterbomb (WB) modules show a larger amount of B faces than A ones (geometric ratios respectively of 0.5 and 0.25). Glide Reflection (GR) is the only pattern that has been designed with a larger amount of A faces than B ones (geometric ratio of 1.5).

Figure shows the distribution of transparent and opaque A and B faces for a Ron Resch (RR) pattern, while Table 1 summarises the optical properties of the four materials adopted for A and B faces. Specular (τ_s) and diffuse (τ_d) transmittance values of translucent materials have been defined according to Addington and Schodek (2005), in analogy with the case of switchable glasses.

The combination of transparent and opaque materials applied to A and B faces gives, therefore, 14 possible semi-transparent configurations for each of the five patterns, in addition to the base cases A0B0, equivalent to a completely transparent device, and A100B100, equivalent to a continuous and perfectly opaque external blind. In order to simulate the dynamic behaviour of the Origami shading, three contraction states of SMA actuators have been considered. C0 corresponds to the closed configuration, C25 corresponds to the open configuration with the SMA reaching the maximum contraction state of 25%, while C10 corresponds to an intermediate condition, with a 10% contraction state applied to the SMA (Figure 6). As a result, 44 configurations (42 intermediate and the two base cases A0B0 and A100B100) have been applied to each of the five Origami patterns.

Evaluation Criteria

A combination of visual comfort and energy indexes has been adopted for the assessment of the shading solution with the best performances under dynamic conditions (i.e. with a variable contraction setting). Galasiu & Reinhart (2008) investigated the main criteria used by designers, engineers and researchers. The vast majority of them (72%) identified energy saving as performance indicator for assessing the overall robustness of the daylighting strategy adopted. Besides, the avoidance of glare was described as the principal objective by all practitioners interviewed.

Within the available metrics to measure glare discomfort, Jakubiec & Reinhart (2012) defined the Daylight Glare Probability (DGP) as "the most robust metric and least prone to produce misleading or inaccurate glare predictions under a variety of analysed solar conditions". DGP and Useful Daylight Illuminance (UDI) have been adopted as the main visual comfort indexes. Indexes have been combined using pass or fail criteria (Reinhart et al. 2006).

DGP represents the probability that a user is disturbed by glare (Wienold and Christoffersen 2006) and is a function of vertical eye illuminance and of luminance gradient of surfaces within the user's visual field. Four glare rating categories can be identified: imperceptible, perceptible, disturbing, and intolerable with upper DGP limits respectively equal to 0.35, 0.40, 0.45, and 0.59 (Wienold 2009). Thus, the four daylight glare comfort classes, DGP_A, DGP_B, DGP_C, and DGP_D for offices proposed by Wienold (2009) have been used. The four classes are defined as follows. For the analyses of daily and monthly variation of Origami patterns:

$$\begin{cases} P_{95\%}\left(DGP(t)\right)\big|_{occupied} \leq 0.35 \wedge \overline{P_{5\%}\left(DGP(t)\right)\big|_{occupied}} \leq 0.38 \Rightarrow DGP_{Class} = DGP_A \\ 0.35 < P_{95\%}\left(DGP(t)\right)\big|_{occupied} \leq 0.40 \wedge 0.38 < \overline{P_{5\%}\left(DGP(t)\right)\big|_{occupied}} \leq 0.42 \Rightarrow DGP_{Class} = DGP_B \\ 0.40 < P_{95\%}\left(DGP(t)\right)\big|_{occupied} \leq 0.45 \wedge 0.42 < \overline{P_{5\%}\left(DGP(t)\right)\big|_{occupied}} \leq 0.53 \Rightarrow DGP_{Class} = DGP_C \\ P_{95\%}\left(DGP(t)\right)\big|_{occupied} > 0.45 \wedge \overline{P_{5\%}\left(DGP(t)\right)\big|_{occupied}} > 0.53 \Rightarrow DGP_{Class} = DGP_D \end{cases} \quad (2)$$

Where $P_{95\%}\left(DGP(t)\right)$ represents the 95th percentile of the hourly calculated values of DGP and $\overline{P_{5\%}\left(DGP(t)\right)}$ represents the average value of the worst 5th percentile of the hourly calculated values of DGP.

For the analyses of hourly variations of Origami patterns, the following definition of DGP classes has been adopted:

$$\begin{cases} DGP \leq 0.35 \Rightarrow DGP_{Class} = DGP_A \\ 0.35 < DGP \leq 0.40 \Rightarrow DGP_{Class} = DGP_B \\ 0.40 < DGP \leq 0.45 \Rightarrow DGP_{Class} = DGP_C \\ DGP > 0.45 \Rightarrow DGP_{Class} = DGP_D \end{cases} \quad (3)$$

UDI is defined as the annual occurrence of illuminance values within a range considered as comfortable by potential users (Nabil and Mardaljevic 2005). The range of useful illuminance values has been calibrated using occupants' surveys in typical office buildings, and values between 100 lx and 3000 lx have been considered as comfortable (Mardaljevic et al. 2012). UDI can be subdivided in two sub-ranges: UDI supplementary (UDI-s) representing the occurrence of illuminance values between 100 lx and 300 lx – for which additional artificial light would be required depending on tasks to be performed –, and UDI autonomous (UDI-a) considering illuminance levels falling within 300-3000 lx range. Moreover, two additional sub-ranges can be identified in order to account for visual discomfort due to hypo-illumination (UDI fell-short – UDI-f – when daylight illuminances are lower than 100 lx), and to hyper-illumination (UDI exceeded – UDI-e – when daylight illuminances exceed 3000 lx).

Annual daylight values have been collected to test the effectiveness of each pattern throughout the year. As previously discussed, fourteen combinations of opacities for the A and B faces have been considered for each of the five selected Origami patterns. Therefore, 70 different patterns have been taken into account. Each of the 70 patterns has been, then, modelled with three SMA actuator's contraction states (0%, 10%, and 25%) in order to account for hourly, daily or monthly dynamic behaviour of the shading. As a result, 210 different configurations have been fully characterised under a daylight and thermal point of view.

Three optimisation conditions have been considered, in order to account for the potential benefits of hourly, daily or monthly variation of the shadings' shape, as already demonstrated in literature (Favoino et al. 2014; Favoino et al. 2015; Kasinalis et al. 2014). Visual comfort criteria have been used to select the optimised actuator's amount of contraction, using the following procedure:

- Glare comfort has been selected as primary criterion and the configurations able to maximize the DGP comfort class have been selected in first instance.
- Among the configurations with DGP comfort maximized, useful illuminance has been selected as secondary criterion. Under this criterion, solutions achieving the highest UDI-a percentage – for monthly and daily variations of configurations – or the lowest spread of indoor illuminance from 1050 lux (mean value of the UDI-a comfort range) – for hourly variations of configurations – have been selected.

After having identified the optimised monthly, daily or hourly profile of contractions for each Origami pattern, on the basis of visual comfort, Total Energy (TE) has been used as the main index for assessing the consequent energy savings. The TE indicator accounts for the sum of site electrical energy required annually by the heating, cooling and artificial lighting systems.

Simulation strategy

Due to the complexity of the shading geometry and the relatively easy management of geometric variables, Origami patterns have been modelled in a parametric environment. Data manipulation, integration with different tools, and simulation capabilities are some of the interesting features of parametric tools. For this purpose, the geometry of the room and of the Origami shading has been generated in Rhinoceros® and parametrically controlled by means of Grasshopper®. Honeybee®, a Grasshopper® plug-in, has been used as the interface with specialised simulation software. Daysim®, a Radiance-based software, has been used as lighting engine. The software is able to compute direct and reflected light and has virtually no limitations in terms of shapes and material properties. However, if non-planar surfaces have to be simulated, the geometric input can cause a crash of the system (Pesenti et al. 2015b). According to Larson et al. (1998), Radiance manipulates geometries assigning to each primitive surface an identifier, used by the program to define a particular material's property. Since Origami patterns are constituted of several faces, to solve the *oconv* tool issue, the continuous surface of the Origami shading device has been imported into Honeybee® as a series of separate planes. All the materials have been chosen within the Radiance material component options provided by Honeybee, and assigned to each face. Radiance reads the translucent material as "a sheet of infinitely thin plastic" (Crone, S., 1992). Translucent materials are not easy to handle especially when combined with a three-dimensional geometry as the Origami one. In order to avoid significant variances, each simulation involving translucent faces has been previously rendered.

After having obtained the optimized pattern of variation of shape by means of daylight simulations, TE values have been predicted, interfacing Honeybee® with EnergyPlus™. In order to account for heat transfer and energy storage, hourly patterns of contraction derived from the

dynamic daylight simulations have been considered. For each Origami configuration and each contraction state of SMAs (0%, 10%, 25%) the value of the average Solar Transmittance (T_{sol}) has been predicted with Daysim. Then, to simplify the geometry and, therefore, computational time spent to perform yearly thermal simulations, external Origami shadings have been modelled as continuous semi-transparent external vertical surfaces placed at a distance of 0.1 m from the window. An hourly-based transparency schedule has been assigned to these external surfaces in order to match the T_{sol} values of the dynamic Origami pattern previously calculated. The solar distribution parameter in EnergyPlus™ has been set to "Full Interior and Exterior with Reflection".

Calibration of daylight simulation parameters

Radiance allows users to set the simulation parameters based on the geometry and on the position or dimensions of elements included in the reference space. A wrong choice of these parameters can greatly affect the final results. Therefore, before starting the simulation processes, a literature review of the Radiance adjustment rendering options was undertaken to set the parameters.

Ambient simulation parameters have proven to affect rendering time and results' accuracy. Five parameters have been selected as critical: ambient bounces (-ab), ambient division (-ad), ambient supersampling (-as), ambient resolution (-ar), ambient accuracy (-aa).

To better explain the process applied, as an example, the error analysis performed to select the most appropriate -ab value to consider is, here, reported.

The Ron Resch pattern in its largest contraction has been considered as modelling case (Figure C25A100B65), and the yearly average indoor illuminance on reference location P1 has been selected as control output. A variation of the -ab parameter from 0 to 8 has been simulated, while keeping all the other indirect ambient values fixed. Figure 7 shows that, after 5 ambient bounces,

the yearly average indoor illuminance steadily converges towards most accurate values. However, it is after 7 ambient bounces that yearly values do not change at all. Therefore, the –ab parameter has been fixed at 7 in the simulations.

Dubois research (2001) highlights two other simulation parameters strictly linked to the -ab one: ambient resolution (-ar) and ambient division (-ad). Ambient division represents the number of rays sent into the sky in order to calculate indirect light, while ambient resolution defines the maximum density of ambient values. Therefore, in order to keep daylight calculations accurate, when a high number of ambient bounces is considered, both ambient resolution and division should be increased. For the scope of the present work –ar has been, therefore, set at 300, while for –ad, a value of 2048 has been assumed.

Finally, ambient accuracy (-aa) and ambient super-samples (-as) represent respectively the maximum error in the indirect irradiance interpolation (currently set to 0.1) and the number of extra rays projected onto sky zones with high luminance variance (currently set to 512).

Analysis of the results

Dynamic behaviour of Origami patterns.

The seventy-two basic Origami patterns (70 cases of patterns with different A and B faces opacities plus the 2 basic cases of completely transparent – A0B0 – and completely opaque surfaces – A100B100 – patterns) have been fully characterized based on yearly calculations. The research methodology started simulating the daylight performance of each pattern configuration in a static way, from 0% to 25% folding states, and from 0% to 100% opacity. Dynamic profiles have been then constructed selecting, for each hour, among the three states of contraction, the one able to optimise the visual behaviour on a yearly basis.

For all Origami variations, DGP (using both $P_{95\%}\big(DGP(t)\big)$ and $\overline{P_{5\%}\big(DGP(t)\big)}$ indexes) has been chosen to be the first metric accounted in the optimisation process. Then, UDI-a has been adopted as secondary optimisation metric. For both metrics (i.e. DGP and UDI-a) no image-based simulation has been performed. Instead, the calculations have used 8760 hourly values of DGP and illuminance levels predicted using the Daysim software.

This has been done in order to define the most promising pattern for each of the five Origami families to further explore and optimise.

The results included in Table 2 show that the best results can be achieved with 100% opacity of A faces and 35% specular transmission of B faces for the Ron Resch (RR), Glide Reflection (GR, GR2), and Miura Ori (MO) families. On the contrary, Waterbomb family performs better when a 35% specular transmission is associated to A faces and 100% opacity is associated to B faces. Moreover, it is worth noting that all configurations with medium-to-medium/high transparency of both A and B faces (i.e. all combinations of A0, A30, A65 with B0, B30, B65) have to be avoided due to excessive glare probabilities ($P_{95\%}\big(DGP(t)\big)$ always equal to 1.0).

From the analysis of Table 2, it is evident how in the majority of cases the solution with the lowest glare probability has also the highest percentage of UDI-a. This is because, despite the three-dimensional shape of the Origami patterns, the use of translucent intermediate states applied to both face A and B lead to levels of illuminance exceeding the maximum threshold of the autonomous range (UDI-a). The only exception is the RR pattern, for which the solution A65B100 has a slightly higher UDI-a than the A100B65 one. However, in this case the latter has been preferred due to significantly lower values of both $P_{95\%}\big(DGP(t)\big)$ and $\overline{P_{5\%}\big(DGP(t)\big)}$.

Optimisation of contraction patterns: influence of monthly, daily and hourly variability

The comparative assessment of the implication on visual comfort and energy savings of hourly, daily or monthly adaptation of shadings' shape has been further explored in this paragraph. This was considered as a useful step in order to understand better how to optimise the numbers of cyclic variations that each of the shadings has to undertake.

Figure 8 shows the five best configurations (one for each Origami geometry) using the three optimization criteria (based respectively on monthly, daily and hourly variations of shapes) for the typical winter and summer weeks in Milan (IT). Preliminarily, it can be noticed that, in almost all cases, the optimised configurations based on monthly, daily and hourly variations of shapes show different patterns. There are several reasons for this occurrence and all depend on the control algorithms used, also reported in equations (2) and (3). While a direct comparison can be made between daily and hourly values – with SMA springs set at the contraction state with the highest occurrence in hourly variations – the same cannot be made between monthly and daily optimization, due to the temporal range considered for monthly optimization, which goes beyond the week represented in Figure 8. It has to be highlighted also that, especially in winter, where the solar radiation incident onto the façade with lower angles, glare issues are amplified, and often monthly optimization is based on the secondary optimization objective (based on illuminance levels), instead on the primary one (based on glare class) as all solutions provide the same glare comfort class (DGP_D).

Analysing the hourly contraction patterns of Figure 8 more in detail, it should be emphasized that MO displays the lowest variation with just 7 hourly movements during the typical winter week and 14 hourly movements during the typical summer one. GR2 pattern, on the contrary shows the highest variation of contraction both in the typical winter week (35 variations) and in the typical summer one (39 variations).

Overall, on a yearly basis, RR and MO are among the patterns with the lowest average daily variations (respectively 2.6 and 2.48), while GR and GR2 need the highest number of average daily variations (respectively 4.16 and 4.52) in the optimised configuration. Moreover, it can be noticed that RR and MO show optimised indoor visual comfort levels when they are in an unfolded position for more than 60% of the time. WB pattern, on the contrary, needs to be in a 25% configuration to achieve a similar result (56% of the year); this is also evident from the analysis of contraction patterns during the selected winter and summer weeks. Respect to other Origami families, the obtuse angles that describes the pineapple like geometry of GR and GR2 patterns lead to a more even distribution throughout the year.

Finally, it can be flagged that the intermediate contraction state (i.e. 10%) is never required for more than 25% of the hours throughout the year, with the only exception of GR2 pattern. Therefore, in a simplified version of the shading, if an hourly optimisation is targeted, the intermediate state could be avoided. On the contrary, if the focus is a daily or monthly variation, an intermediate step of contraction can be beneficially used.

Visual comfort analyses

Table 3 presents the detailed daylight comfort assessment, based on P1 location. It accounts for all the three time spans previously defined (i.e. hourly, daily, monthly shape variations). Together with the two DGP metrics, full UDI values are proposed here for a complete assessment of the distribution of natural light in the room.

From the analyses of data presented in the table, it is visible how the geometry and the combination of materials played a significant role in achieving visual comfort requirements. Opaque surfaces are needed to increase the shading effect, while translucent materials with low

specular light transmittance can mitigate glare, while maintaining a certain degree of view towards the outside.

By the comparison of hourly control with daily or monthly one, it can be observed that a better management of the direct solar radiation and better results in terms of glare reduction can be achieved. However, it has to be noted that three patterns (RR, GR, and GR2) do not fall into any of the Wienold comfort classes (Wienold 2009). The other two (MO and WB) fall respectively into the Reasonable class (C) and the Best one (A). Under an indoor illuminance viewpoint, all the patterns show a very good behaviour, with UDI-a criteria constantly met for over 74% of the time. It can be highlighted that, during the remaining percentage of time, indoor illuminances are generally below 300 lx (sum of UDI-f and UDI-s percentages), even though GR and GR2 patterns show relatively high UDI-e values.

By adopting a daily control of Origami shape, DGP values rise over the maximum thresholds for class C for all the patterns. WB shows the best behaviour thanks to $P_{95\%}\big(DGP(t)\big)$ of 0.36. However, as $\overline{P_{5\%}\big(DGP(t)\big)}$ is beyond the upper limit for class C (0.53), WB pattern still must be classified within glare comfort class D. On the contrary, a similar decrease in comfort levels cannot be found if UDI-a metric is considered. In fact, as an average, UDI-a values show a decrease of only 1.6%. Similar patterns can be found for all UDI sub-ranges as well.

Moving from a daily to a monthly optimisation, glare probabilities do not show significant changes. The only notable exception is represented by WB pattern, which experiences a significant increase of both $P_{95\%}\big(DGP(t)\big)$ and $\overline{P_{5\%}\big(DGP(t)\big)}$ values (increasing of about 64%, if compared to daily optimised patterns). Monthly optimisation produces also a reduction of UDI-a values (average decrease of about 3% if compared to daily optimisation and of about 4.6% if compared to the hourly one).

From the visual comfort analyses, we can conclude that the selection of shading patterns is strictly correlated to the two visual comfort criteria (glare or illuminance) and to the order in which they are applied. An optimisation based on criteria based only on glare assessment can, indeed, produced unwanted results in terms of indoor illuminances.

Prediction of total energy savings

To complement the presented daylight analyses, the implication of Origami patterns selection on the thermal performance of the indoor space was assessed. Envelope's properties have been based on the most restrictive n-ZEB requirements. Therefore, this has consequences on cooling and heating loads and on the sensitivity of the model to internal and solar gains. As previously discussed, Total Energy (TE) has been selected as metric for the assessment of efficacy of shadings' patterns optimisations. Moreover, to account for the variation of contraction states, artificial lighting and transparency schedules have been set up into the thermal model according to the dynamic daylighting profiles previously obtained.

Table 4 includes the calculation of TE for the five selected patterns. TE is presented in terms of its three major components (Cooling, Heating and Artificial Lighting). It is worth noting that TE is mostly affected by lighting consumption for all patterns and that heating demands are almost inexistent, and therefore not affected by optimisation strategies. Comparable results can be found in literature for n-ZEB buildings of similar use located in even colder climates. Ascione et al. (2016) demonstrated that in a net zero-energy office building in Berlin heating load is about 6% of the total specific electric energy use of the building. Similarly, a recent study performed by Jung et al. (2018) showed that, by adopting n-ZEB standards in office buildings in London, space heating is almost reduced to zero.

As an average, optimisation criteria produce a variation of total energy consumption of less than 10%. Therefore, under a thermal perspective a very sophisticated hourly variation of the geometry may not be worth pursuing. Moreover, some of the patterns show no (GR and GR2) or very little (WB) variation of TE moving from an hourly to a monthly variation of geometry. MO patterns experience even a decrease in their energy performance moving from occasional monthly movements to frequent hourly ones. RR pattern represent the only notable exception, experiencing substantial energy savings adopting hourly variations profiles (about 24 kWh/m^{2}y of savings comparing monthly with hourly patterns). Following the results, Ron Resch pattern can represent the idea of a shading device that regulates hour by hour its geometry so as to manage the incoming radiation, leading to more stable indoor comfort conditions throughout the year.

Overall, concentrating the analysis on the hourly-optimised profiles, with a TE of 42.5 kWh/m^{2}y, the RR pattern shows the most promising geometry, followed by GR and GR2 ones (both with TE around 50 kWh/m^{2}y), and by MO and WB Origami families (both with TE around 60 kWh/m^{2}y). The variation of performance of different origami families can be largely attributed to artificial lighting consumptions. It is interesting to note that from the precedent visual comfort analysis, natural light levels do not experience similar variations. This is a demonstration that results of visual and thermal analyses should be read in conjunction in order to find the most suitable high performing technical solution.

If daily and monthly-optimised patterns are analysed, it can be noticed that GR, GR2 and MO families perform very similarly, with TE around 50 kWh/m^{2}y, while RR and WB patterns show energy demands between 61 and 68 kWh/m^{2}y. Again, also in this last case, variations of energy demand largely depend on the artificial lighting consumptions.

Pilot experimental study: development of the KUMORIgami prototype

In order to determine the technological issues related to the design and construction of an Origami shading, as well as the practical challenges in actuating the change of shape through SMAs, a prototype – named KUMORIgami as follows – has been produced and is here presented. The prototype complements, also, the theoretical analyses based on simulations included in previous paragraphs. The early-stage prototype translates the RRA100B65 pattern into a shading concept that deploys thanks to SMA springs and manages the incoming daylight by combining translucent and opaque faces. Besides, the selected Origami pattern was easy to implement and allowed to stretch the SMA actuators up to their maximum length (165 mm) optimizing the folding rate of the shading component. KUMORIgami is composed of modular panels with an isosceles triangular shape (475 mm each side), which have been produced by laser cutting a translucent polypropylene (PP) sheet. The panel has been then slightly carved and folded by hand. PP has been demonstrated to be have a high fatigue strength, making it feasible to perform several sequences of movement. Beyond the triangular module of the pattern, the laser cut has been used to cut opaque Perspex triangle for the A faces, and to pierce small holes for attaching to the panel the SMA springs (Figure 9). Placed along the outer vertexes, the 6 actuators create a hexagon, and with this pattern the linear contraction of each spring results in a multidirectional deployment of the shading.

In order to activate the shape, the springs have been connected with copper tape reinforced with an aluminium wire. The circuit has been closed by "crocodile clips" linked to a power supply. The hexagon contraction started in between 8.4 – 9 V and 2 A. The full contraction of the Origami module happened with a current voltage of 11 V, and therefore with an electric power of about 24 W.

Without any external constraint, the mock-up shows a folding rate of 26%. However, this contraction decreases when each SMA spring is linked to a bias spring, needed to take back the SMA spring to its initial length when low temperatures are reached. RR pattern has been fixed through these springs to a triangular wooden structure (500 mm of side length) as shown in Figure 10. Step by step, Ron Resch prototype has been linked to different tension springs, searching for the ones allowing the SMA spring contraction, while impressing the minimum stress to unfold the Origami surface. Three aluminium springs have been selected, the bottom two with an elastic coefficient (k) of 0.06 N/mm and the top one with k = 0.5 N/mm. Once the frame and the springs have been applied to the Origami, it has been found a final folding rate of 20%, with a total decrement due to external restraints of about 6%.

Conclusions

The ability of Origami surface to fold following the imposed requirements, their versatility in terms of space and their multi-faced nature, which allows envisioning infinite possibilities are some of the features that make these shapes adaptive by nature. Albeit several studies refer to Origami as a generative technique, in architecture they are still underexplored, especially in the field of kinetic envelopes.

In order to achieve a kinetic system, the Origami geometry has been called to physically respond to the environment using SMAs micro-actuators, as to optimise the levels of incoming daylight. The kinetic potential has been tested with new digital tools to investigate their movement. Dynamic simulations have been performed to define the best among the patterns to be further explored with in-depth analyses. With a variety of behaviours displayed by their 3D nature and the use of SMAs micro actuators, the materials' trend seems to be a pattern to follow in order to attain a possible layout of the shading device. Mixing different percentages of transparency delivers better

performances; this has been achieved in the present study creating two groups of faces for each pattern. The results show that at least one of the two faces must be completely opaque to achieve a good visual and thermal performance. However, the overall performance seems not to be affected by the relative proportion between the two faces. For instance, GR and MO patterns perform very similarly, even though they have different geometric ratios between transparent and opaque faces. Instead, visual and thermal behaviour must be related more to the geometric configuration of each pattern in planar and contracted shape. By analysing the results, it can be acknowledged that a gradual expansion or contraction of the shape could deliver interesting results, especially when a daily or monthly variation is considered. The research uses market available SMAs that, when actuated, contract instantaneously, going from martensitic state to the austenitic one.

With the aim of understanding issues and physical restrictions related to the opening mechanism and to the integration of SMAs in the adaptive origami shadings, the paper introduces KUMORIgami, an early-stage prototype based on Ron Resch pattern. When the prototype is attached to external restraints placed at the edges of the shading, the reduction of area exhibited by the digital model when contracted decreases of about 6%, leading to an overall folding rate of 20%.

The method developed suggests an alternative approach to design responsive shading components. To guarantee the daylighting levels exploited in the evaluation criteria and to improve on the visual comfort conditions presented under direct sunlight conditions and inferred by the literature review, the combination and makeup of Origami shapes and SMAs should be improved. Besides, further experimental studies should be carried out in order to determine the behaviour of the shading when subject to real-time environmental conditions, exploiting new materials and techniques.

References

Addington, M., and Schodek, D. L. (2005). *Smart Materials and New Technologies for the architecture and design professionals*, Architectural Press - Elsevier, Oxford (U.K.).

Adriaenssens, S., Rhode-Barbarigos, L., Kilian, A., Baverel, O., Charpentier, V., Horner, M., and Buzatu, D. (2014). "Dialectic form finding of passive and adaptive shading enclosures." *Energies*, 7(8), 5201-5220.

Aedas (2012). "Al Bahar Towers." <www.aedas.com>. (14/08/2015).

Ascione, F., Bianco, N., Böttcher, O., Kaltenbrunner, R., and Vanoli, G. P. (2016). "Net zero-energy buildings in Germany: Design, model calibration and lessons learned from a case-study in Berlin." *Energy and Buildings*, 133, 688-710.

Baetens, R., Jelle, B. P., and Gustavsen, A. (2010). "Properties, requirements and possibilities of smart windows for dynamic daylight and solar energy control in buildings: A state-of-the-art review." *Solar Energy Materials and Solar Cells*, 94(2), 87-105.

Cammarano, S., Pellegrino, A., Lo Verso, V. R. M., and Aghemo, C. (2015). "Assessment of daylight in rooms with different architectural features." *Building Research and Information*, 43(2), 222-237.

Cheng, N. (2012a). "Petal Variations: Surfaces for Light and Shadow Effects." *Shape Modeling International 2012*College Station, Texas, USA.

Cheng, N., Rodriguez, A. N., and Koger, A. B. (2012b). "Folded Sun-Shades: from Origami to Architecture." *ACSA 100th Annual Meeting*Boston, MA.

Dubois, M.-C. (2001). "Impact of Shading Devices on Daylight Quality in Offices." Lund University.

European Union (2010). "Directive 2010/31/EU of the European Parliament and of the Council of 19 May 2010 on the energy performance of buildings (recast)." Official Journal of the European Union.

Favoino, F., Jin, Q., and Overend, M. "Towards an ideal adaptive glazed façade for office buildings." *Proc., 6th International Conference on Sustainability in Energy and Buildings, SEB 2014*, Elsevier Ltd, 289-298.

Favoino, F., Overend, M., and Jin, Q. (2015). "The optimal thermo-optical properties and energy saving potential of adaptive glazing technologies." *Applied Energy*, 156(0), 1-15.

Fiorito, F., Sauchelli, M., Arroyo, D., Pesenti, M., Imperadori, M., Masera, G., and Ranzi, G. (2016). "Shape morphing solar shadings: A review." *Renewable and Sustainable Energy Reviews*, 55, 863-884.

Goia, F., Haase, M., and Perino, M. (2013). "Optimizing the configuration of a façade module for office buildings by means of integrated thermal and lighting simulations in a total energy perspective." *Applied Energy*, 108, 515-527.

Goia, F., Perino, M., and Serra, V. (2014). "Experimental analysis of the energy performance of a full-scale PCM glazing prototype." *Solar Energy*, 100, 217-233.

Granqvist, C. G. (2002). "Smart windows and intelligent glass façades." *Smart Materials Bulletin*(10), 9-10.

Hammad, F., and Abu-Hijleh, B. (2010). "The energy savings potential of using dynamic external louvers in an office building." *Energy and Buildings*, 42(10), 1888-1895.

Italy (2013). "Legislative Decree 4 June 2013 nr. 63."

Janssen, R. (2004). "Towards Energy Efficient Buildings in Europe." EuroACE, The European Alliance of Companies for Energy Efficiency in Buildings, London.

Jelle, B. P., Hynd, A., Gustavsen, A., Arasteh, D., Goudey, H., and Hart, R. (2012). "Fenestration of today and tomorrow: A state-of-the-art review and future research opportunities." *Solar Energy Materials and Solar Cells*, 96(1), 1-28.

Jin, Q., and Overend, M. (2014). "Sensitivity of façade performance on early-stage design variables." *Energy and Buildings*, 77, 457-466.

Jones, P., Hou, S. S., and Li, X. (2015). "Towards zero carbon design in offices: Integrating smart facades, ventilation, and surface heating and cooling." *Renew. Energy*, 73, 69-76.

Jung, N., Paiho, S., Shemeikka, J., Lahdelma, R., and Airaksinen, M. (2018). "Energy performance analysis of an office building in three climate zones." *Energy and Buildings*, 158, 1023-1035.

Kasinalis, C., Loonen, R. C. G. M., Cóstola, D., and Hensen, J. L. M. (2014). "Framework for assessing the performance potential of seasonally adaptable facades using multi-objective optimization." *Energy and Buildings*, 79, 106-113.

Kolokotsa, D., Rovas, D., Kosmatopoulos, E., and Kalaitzakis, K. (2011). "A roadmap towards intelligent net zero- and positive-energy buildings." *Solar Energy*, 85(12), 3067-3084.

Koo, S. Y., Yeo, M. S., and Kim, K. W. (2010). "Automated blind control to maximize the benefits of daylight in buildings." *Building and Environment*, 45(6), 1508-1520.

Larson, G. W., Shakespeare, R., Ehrilich, C., Mardaljevic, J., Phillips, E., and Apian-Bennewitz, P. (1998). *Rendering with Radiance: the art and science of lighting visualization*, Morgan Kaufmann, San Francisco, CA.

Lee, E. S., DiBartolomeo, D. L., Rubinstein, F. M., and Selkowitz, S. E. (2004). "Low-cost networking for dynamic window systems." *Energy and Buildings*, 36(6), 503-513.

Lienhard, J., Schleicher, S., Poppinga, S., Masselter, T., Milwich, M., Speck, T., and Knippers, J. (2011). "Flectofin: A hingeless flapping mechanism inspired by nature." *Bioinspiration and Biomimetics*, 6(4).

Lohnert, G., Dalkowski, A., and Sutter, W. (2003). "Integrated Design Process. A Guideline for Sustainable and Solar-Optimised Building Design." IEA - SHC Programme.

Lollini, R., Danza, L., and Meroni, I. (2010). "Energy efficiency of a dynamic glazing system." *Solar Energy*, 84(4), 526-537.

Loonen, R. C. G. M., Singaravel, S., Trčka, M., Cóstola, D., and Hensen, J. L. M. (2014). "Simulation-based support for product development of innovative building envelope components." *Autom Constr*, 45, 86-95.

Loonen, R. C. G. M., Trčka, M., Cóstola, D., and Hensen, J. L. M. (2013). "Climate adaptive building shells: State-of-the-art and future challenges." *Renewable and Sustainable Energy Reviews*, 25, 483-493.

Malara, F., Cannavale, A., Carallo, S., and Gigli, G. (2014). "Smart windows for building integration: A new architecture for photovoltachromic devices." *ACS Appl. Mater. Interfaces*, 6(12), 9290-9297.

Manzan, M., and Padovan, R. (2015). "Multi-criteria energy and daylighting optimization for an office with fixed and moveable shading devices." *Adv. Build. Energy Res.*

Mardaljevic, J., Andersen, M., Roy, N., and Christoffersen, J. (2012). "Daylighting metrics: is there a relation between Useful Daylight Illuminance and Daylight Glare Probability?" *Building Simulation and Optimization Conference BSO12*Loughborough, UK.

Nabil, A., and Mardaljevic, J. (2005). "Useful daylight illuminance: A new paradigm for assessing daylight in buildings." *Lighting Research and Technology*, 37(1), 41-59.

Naboni, E. (2014). "Integration of Outdoor Thermal and Visual Comfort in Parametric Design." *Passive and Low-Energy Architecture International Conference*Ahmedabad (India).

Nespoli, A., Besseghini, S., Pittaccio, S., Villa, E., and Viscuso, S. (2010). "The high potential of shape memory alloys in developing miniature mechanical devices: A review on shape memory alloy mini-actuators." *Sensors and Actuators, A: Physical*, 158(1), 149-160.

Nielsen, M. V., Svendsen, S., and Jensen, L. B. (2011). "Quantifying the potential of automated dynamic solar shading in office buildings through integrated simulations of energy and daylight." *Solar Energy*, 85(5), 757-768.

Osório, F., Paio, A., and Oliveira, S. "KOS- kinetic origami surface." *Proc., 19th International Conference on Computer-Aided Architectural Design Research in Asia - Rethinking Comprehensive Design: Speculative Counterculture, CAADRIA 2014*, The Association for Computer-Aided Architectural Design Research in Asia (CAADRIA), 201-210.

Pacheco, R., Ordóñez, J., and Martínez, G. (2012). "Energy efficient design of building: A review." *Renewable and Sustainable Energy Reviews*, 16(6), 3559-3573.

Pesenti, M., Masera, G., and Fiorito, F. (2015b). "Shaping an Origami Shading Device through Visual and Thermal Simulations." *Energy Procedia*, 78, 346-351.

Pesenti, M., Masera, G., Fiorito, F., and Sauchelli, M. (2015a). "Kinetic Solar Skin: A Responsive Folding Technique." *Energy Procedia*, 70(0), 661-672.

Reinhart, C. F., Mardaljevic, J., and Rogers, Z. (2006). "Dynamic daylight performance metrics for sustainable building design." *LEUKOS. J. Illum. Eng. Soc.*, 3(1), 7-31.

Sartori, I., Napolitano, A., and Voss, K. (2012). "Net zero energy buildings: A consistent definition framework." *Energy and Buildings*, 48, 220-232.

Suralkar, R. "Solar Responsive Kinetic Facade Shading Systems inspired by plant movements in nature." *Proc., People and Buildings*.

Tzempelikos, A., and Athienitis, A. K. (2007). "The impact of shading design and control on building cooling and lighting demand." *Solar Energy*, 81(3), 369-382.

UNI (1995). "10339: 1995. Aeraulic systems designed to provide comfort. General information, classification and requirements. Rules for quotes, offers, orders and supply." Italian organization for Standardization (UNI), Milan (IT).

van Dijk, D. (2002). "Thermal and solar modelling and characterisation; the role of IEA SHC Task 27." International Energy Agency, Solar Heating and Cooling Programme.

Wang, J., Beltrán, L. O., and Kim, J. "From static to kinetic: A review of acclimated kinetic building envelopes." 4022-4029.

Wienold, J. "Dynamic daylight glare evaluation." *Proc., 11th International IBPSA Conference - Building Simulation 2009, BS 2009*, 944-951.

Wienold, J., and Christoffersen, J. (2006). "Evaluation methods and development of a new glare prediction model for daylight environments with the use of CCD cameras." *Energy and Buildings*, 38(7), 743-757.

Figures

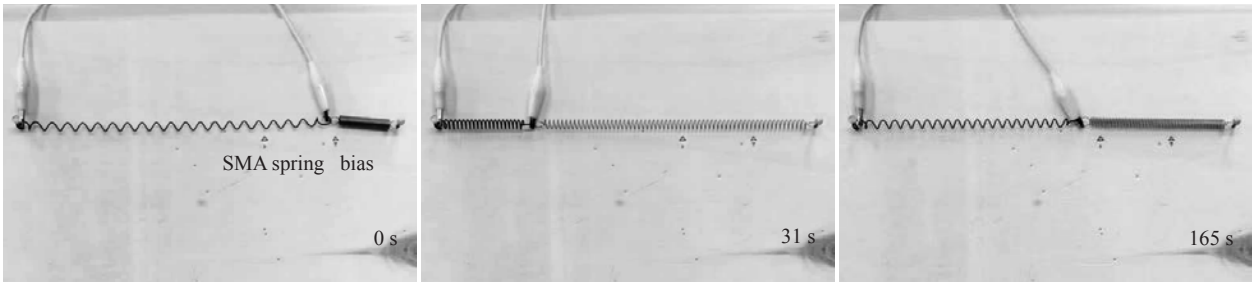

Figure 1. The shape memory alloy spring is activated using a power supply. At the bottom right of each image the time of contraction and then elongation is displayed.

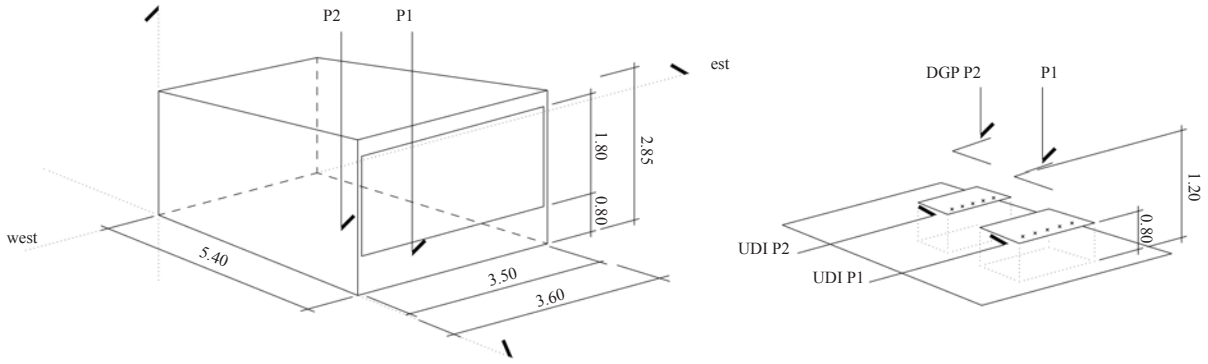

Figure 2. (a) Geometry of reference room and position of sensor points P1 and P2; (b) Details of sensor points P1 and P2 for illuminance and glare calculations.

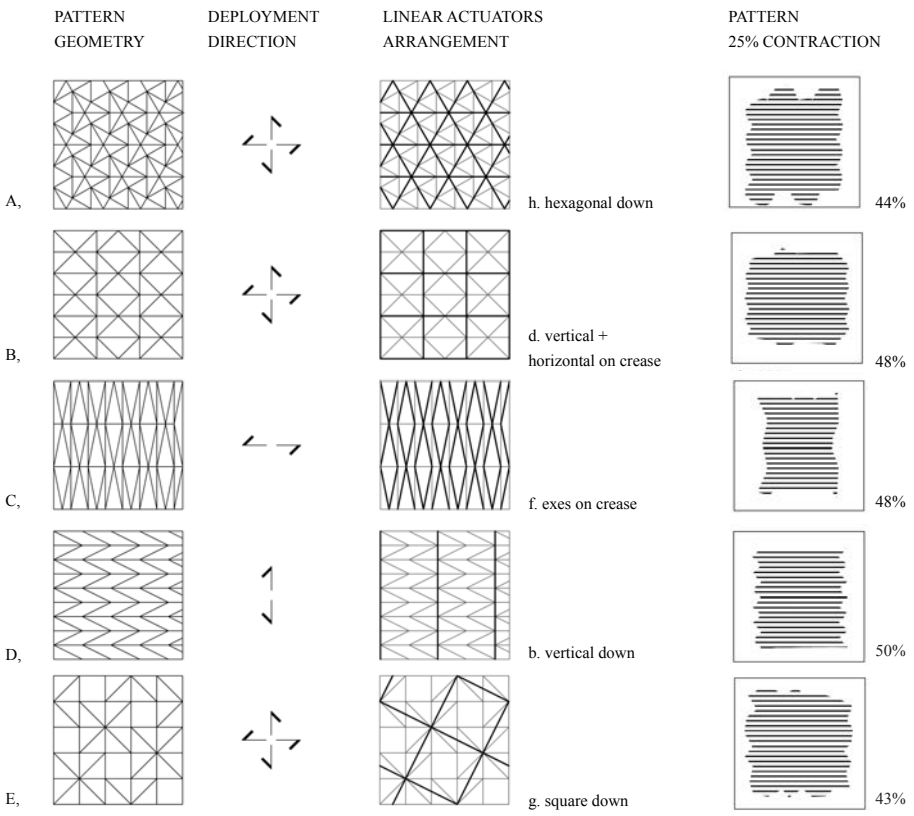

Figure 3. Deployable patterns of five selected Origami families: Ron Resch (RR), Glide Reflection (GR, GR2), Miura Ori (MO), Waterbomb (WB)

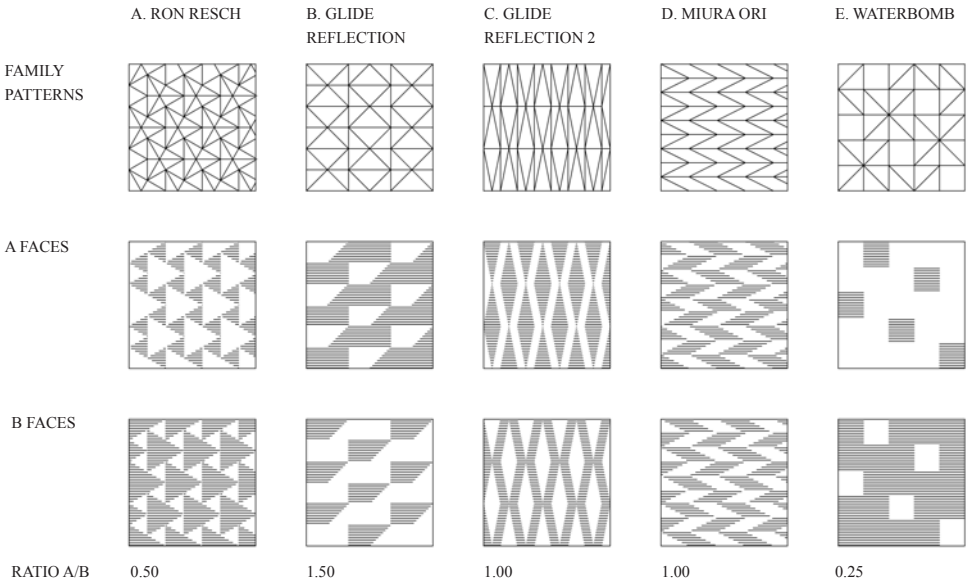

Figure 4. Definition of A and B faces

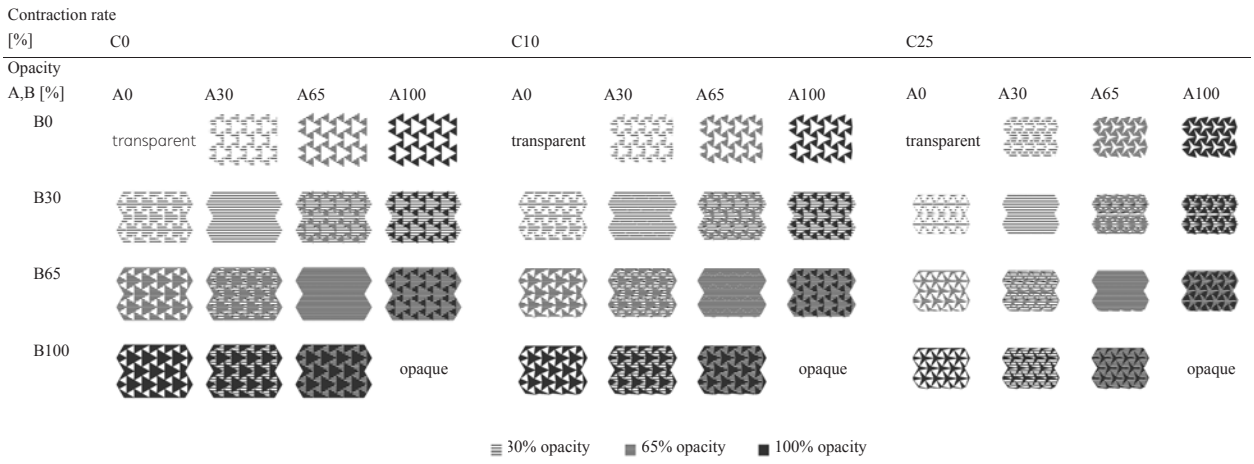

Figure 5. Forty-four configurations of shadings: no shading (A0; B0), complete shading (A100; B100) and mixed combinations of opacity for the A and B faces, each for a specific rate of contraction.

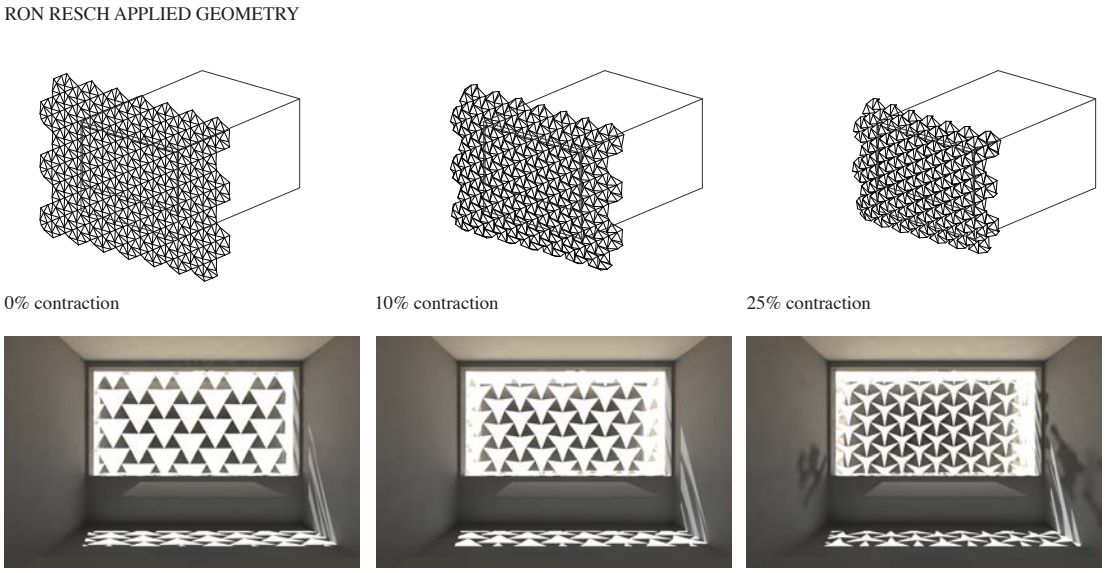

Figure 6. Axonometric view and perspective view from the interior of RRA100B0 shading for the three contraction states.

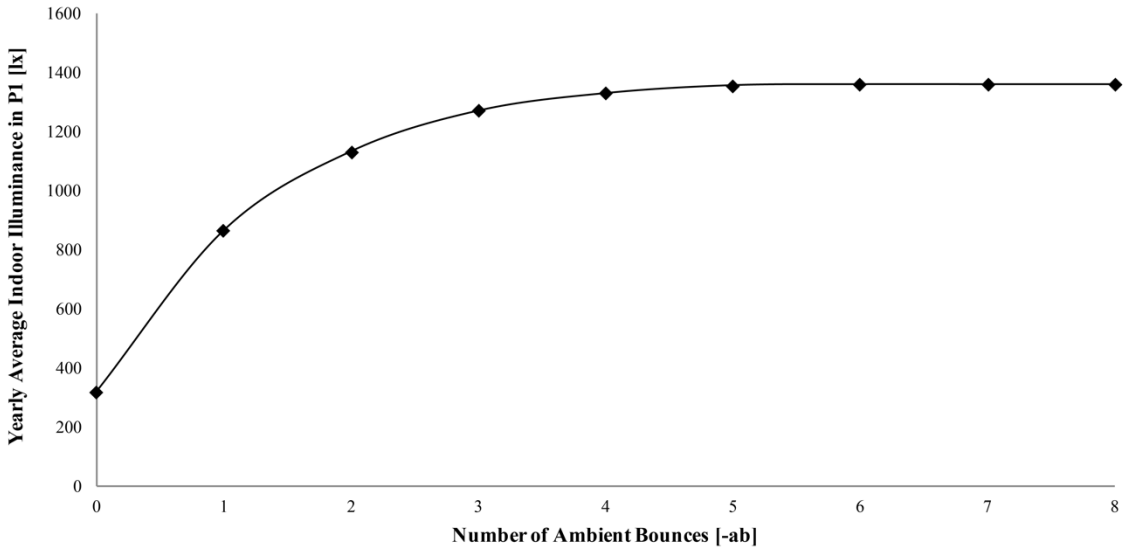

Figure 7. Error analysis for setting up “ambient bounces” simulation parameter.

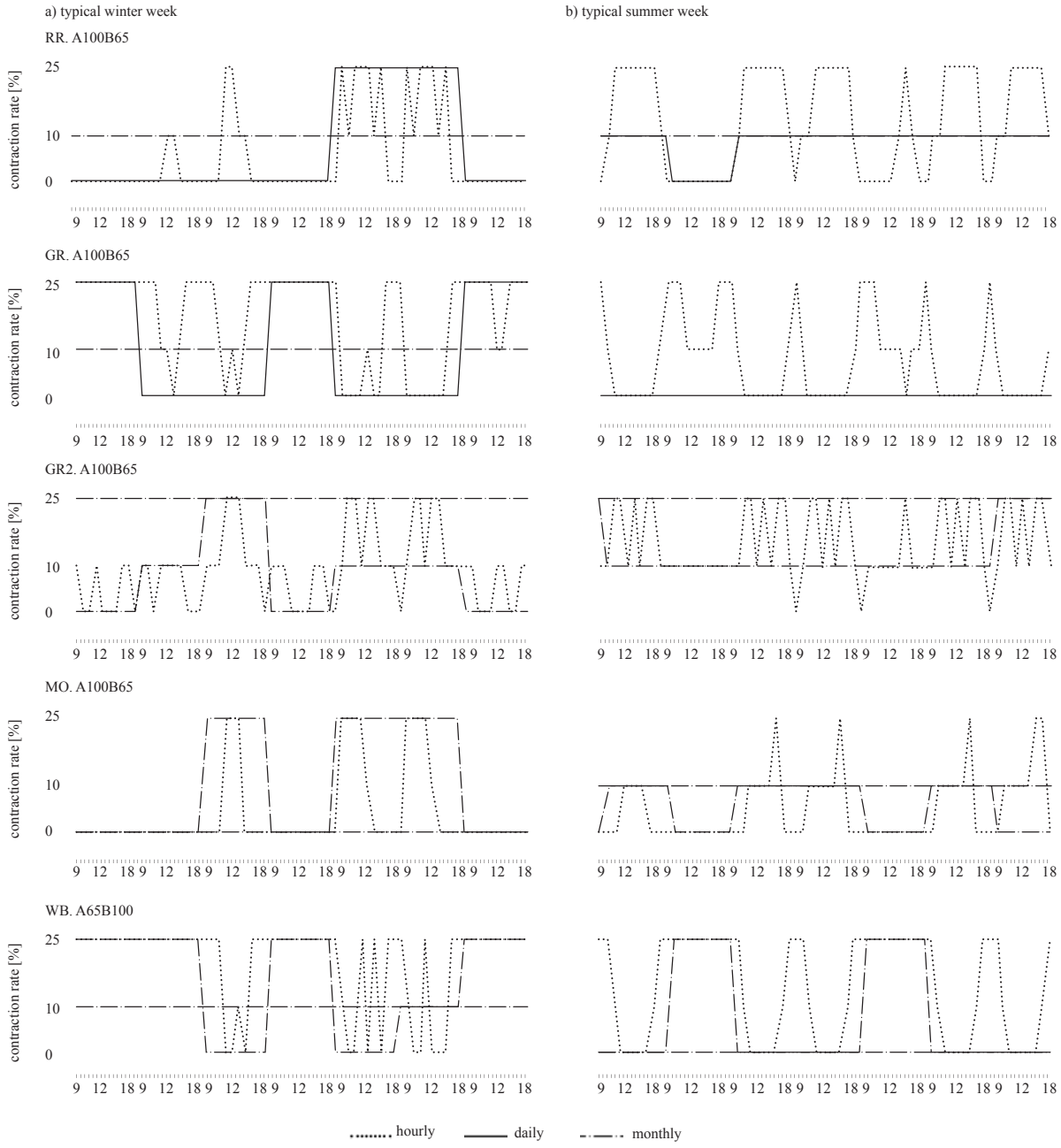

Figure 8. Optimisation of contraction states on hourly (dots), daily (continuous) and monthly (dash-dots) scale for the five selected patterns; a) typical winter week, b) typical summer week.

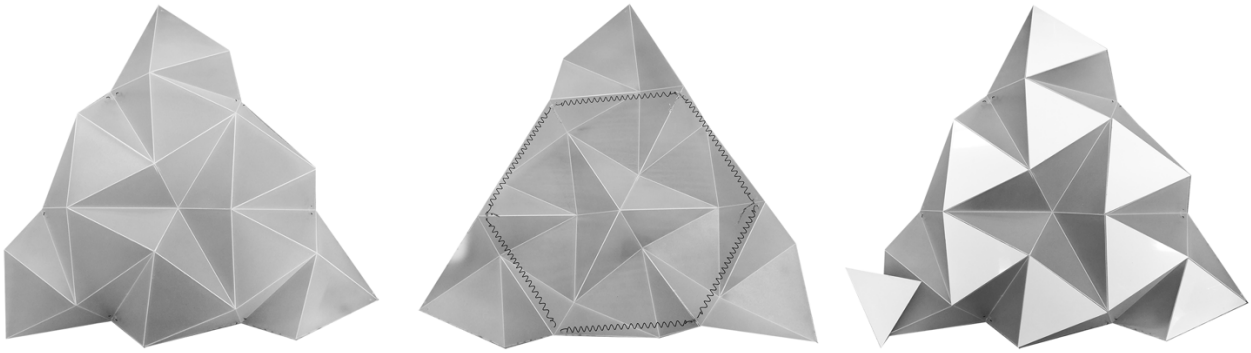

Figure 9. KUMORIgami: the module cut out with a laser cut following its geometry definition, the SMA springs arrangement and its face characterisation made with two different plastic materials (white for A faces and translucent for B faces).

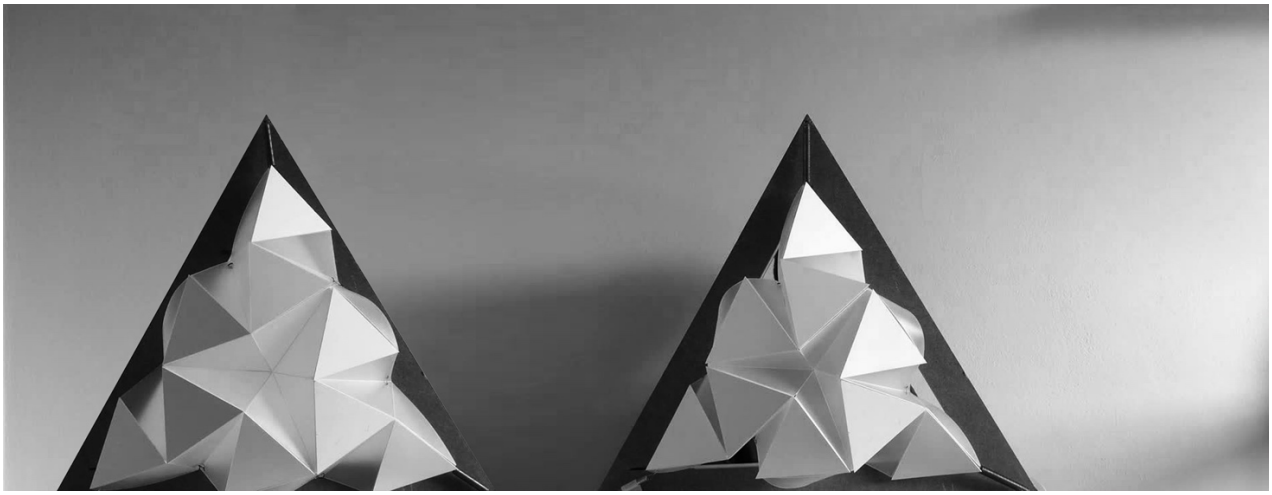

Figure 10. KUMORIgami with bias springs actuated with power supply. (a) the initial configuration and (b) the final shape highlighting a surface reduction of 20%

Tables

Table 1: Optical properties of materials adopted for A and B faces.

Code	R	S	ρ	τ_s	τ_d
0	-	-	-	1.00	0.00
30	-	-	-	0.70	0.25
65	-	-	-	0.35	0.25
100	0.68	0.01	0.01	0.00	0.00

Table 2: yearly behaviour of Origami patterns. Results expressed in terms of $DGP_{95\%}/DGP_{5\%ave}$ (UDI-a)

Origami families	Faces' combinations	A0	A30	A65	A100
RR	**B0**	1.00/1.00 (38.3)	1.00/1.00 (40.3)	1.00/1.00 (54.9)	1.00/1.00 (52.4)
	B30	1.00/1.00 (48.9)	1.00/1.00 (40.8)	1.00/1.00 (56.4)	1.00/1.00 (63.8)
	B65	1.00/1.00 (49.6)	1.00/1.00 (54.9)	1.00/1.00 (60.9)	**0.47/0.71 (75.3)**
	B100	1.00/1.00 (68.8)	0.77/0.95 (71.8)	0.65/0.77 (78.2)	N/A*
GR	**B0**	1.00/1.00 (38.3)	1.00/1.00 (40.6)	1.00/1.00 (47.9)	0.92/0.99 (64.3)
	B30	1.00/1.00 (39.8)	1.00/1.00 (41.3)	1.00/1.00 (53.3)	0.87/0.97 (64.5)
	B65	1.00/1.00 (45.2)	1.00/1.00 (52.4)	1.00/1.00 (53.2)	**0.42/0.64 (78.3)**
	B100	1.00/1.00 (51.2)	1.00/1.00 (52.5)	0.95/0.99 (65.3)	N/A*
GR2	**B0**	1.00/1.00 (38.3)	1.00/1.00 (40.5)	1.00/1.00 (47.0)	1.00/1.00 (58.2)
	B30	1.00/1.00 (40.4)	1.00/1.00 (42.2)	1.00/1.00 (53.8)	0.90/0.99 (61.7)
	B65	1.00/1.00 (47.8)	1.00/1.00 (56.8)	1.00/1.00 (52.9)	**0.67/0.80 (74.6)**
	B100	0.97/0.99 (52.8)	0.93/0.99 (58.0)	0.70/0.84 (66.3)	N/A*
MO	**B0**	1.00/1.00 (38.3)	1.00/1.00 (39.8)	1.00/1.00 (52.5)	0.57/0.86 (74.1)
	B30	1.00/1.00 (41.2)	1.00/1.00 (41.4)	1.00/1.00 (57.3)	0.49/0.78 (76.4)
	B65	1.00/1.00 (45.4)	1.00/1.00 (57.3)	1.00/1.00 (54.5)	**0.35/0.44 (74.8)**
	B100	1.00/1.00 (47.8)	1.00/1.00 (46.2)	0.86/0.98 (60.7)	N/A*
WB	**B0**	1.00/1.00 (38.3)	1.00/1.00 (39.6)	1.00/1.00 (43.0)	1.00/1.00 (46.7)
	B30	1.00/1.00 (40.5)	1.00/1.00 (41.2)	1.00/1.00 (55.0)	1.00/1.00 (46.5)
	B65	1.00/1.00 (50.8)	1.00/1.00 (54.5)	1.00/1.00 (54.5)	1.00/1.00 (61.9)
	B100	0.35/0.41 (68.7)	0.34/0.38 (71.1)	**0.31/0.36 (78.0)**	N/A*

Note: the best combinations are in bold.
*no daylight source inside due to the totally opaque shading device configuration.

Table 3. DGP and UDI values displayed for no shading configuration (A0B0), totally opaque configuration (A100B100) and for the five most promising dynamic patterns.

Shape's variability	Metric	A0B0	RR. A100B65	GR. A100B65	GR2. A100B65	MO. A100B65	WB. A65B100	A100B100
Hourly	$DGP_{95\%}$	1.0	0.47	0.42	0.67	0.35	0.31	0.0*
	$DGP_{5\%\ ave}$	1.0	0.71	0.64	0.80	0.44	0.36	0.0*
	UDI-f	4.8	11.6	7.3	9.8	11.9	10.1	100.0*
	UDI-s	3.6	12.0	4.9	8.3	12.6	9.8	0.0*
	UDI-a	38.3	75.3	78.3	74.6	74.8	78.0	0.0*

	UDI-e	53.2	1.2	9.5	7.3	0.7	2.1	0.0*
Daily	$DGP_{95\%}$	1.0	0.66	0.61	0.73	0.54	0.36	0.0*
	$DGP_{5\%\ ave}$	1.0	0.82	0.72	0.64	0.69	0.58	0.0*
	UDI-f	4.8	11.9	9.2	9.9	12.2	11.0	100.0*
	UDI-s	3.6	12.0	5.8	8.4	13.3	10.8	0.0*
	UDI-a	38.3	73.4	75.5	74.1	73.9	76.1	0.0*
	UDI-e	53.2	2.6	9.6	7.6	0.6	2.1	0.0*
Monthly	$DGP_{95\%}$	1.0	0.66	0.63	0.74	0.59	0.59	0.0*
	$DGP_{5\%\ ave}$	1.0	0.83	0.76	0.87	0.70	0.76	0.0*
	UDI-f	4.8	11.8	10.9	9.9	12.8	11.2	100.0*
	UDI-s	3.6	12.2	10.2	8.9	13.6	13.1	0.0*
	UDI-a	38.3	72.7	68.8	73.1	70.7	72.6	0.0*
	UDI-e	53.2	3.3	10.1	8.1	2.9	2.8	0.0*

* no daylight source inside due to the totally opaque shading device configuration.

Table 4. TE values for the five selected dynamic patterns.

Shape's variability	**Shading Configurations**	**RR.A100B65**	**GR.A100B65**	**GR2.A100B65**	**MO.A100B65**	**WB.A65B100**
Hourly	Cooling [kWh/m^{2}y]	16.0	18.4	18.5	21.0	22.2
	Heating [kWh/m^{2}y]	0.1	0.1	0.1	0.1	0.1
	Lighting [kWh/m^{2}y]	26.4	32.6	30.3	36.2	39.8
	Total [kWh/m^{2}y]	42.5	51.1	48.9	57.3	62.0
Daily	Cooling [kWh/m^{2}y]	21.2	18.3	19.1	19.3	23.7
	Heating [kWh/m^{2}y]	0.1	0.1	0.1	0.1	0.0
	Lighting [kWh/m^{2}y]	40.0	32.5	32.0	32.6	44.5
	Total [kWh/m^{2}y]	61.2	50.8	51.2	51.9	68.3
Monthly	Cooling [kWh/m^{2}y]	22.8	18.3	18.3	19.3	23.2
	Heating [kWh/m^{2}y]	0.1	0.1	0.1	0.1	0.0
	Lighting [kWh/m^{2}y]	43.6	32.7	30.3	32.5	43.2
	Total [kWh/m^{2}y]	66.5	51.1	48.7	51.8	66.4